Published in final edited form as:
Cell. 2012 January 20; 148(1-2): 59–71. doi:10.1016/j.cell.2011.12.013.

Genome Sequencing of Pediatric Medulloblastoma Links Catastrophic DNA Rearrangements with *TP53* Mutations

Tobias Rausch[1,*], **David T.W. Jones**[2,*], **Marc Zapatka**[2,*], **Adrian M. Stütz**[1,*], **Thomas Zichner**[1], **Joachim Weischenfeldt**[1], **Natalie Jäger**[3], **Marc Remke**[2,4], **David Shih**[5], **Paul A. Northcott**[5], **Elke Pfaff**[2], **Jelena Tica**[1], **Qi Wang**[4], **Luca Massimi**[6], **Hendrik Witt**[2,4], **Sebastian Bender**[2,4], **Sabrina Pleier**[2,4], **Huriye Cin**[2], **Cynthia Hawkins**[5,7], **Christian Beck**[4], **Andreas von Deimling**[8], **Volkmar Hans**[9], **Benedikt Brors**[3], **Roland Eils**[3], **Wolfram Scheurlen**[10], **Jonathon Blake**[1], **Vladimir Benes**[1], **Andreas E. Kulozik**[4], **Olaf Witt**[4,11], **Dianna Martin**[12], **Cindy Zhang**[12], **Rinnat Porat**[12], **Diana Merino**[12], **Jonathan Wasserman**[12], **Nada Jabado**[13], **Adam Fontebasso**[13], **Lars Bullinger**[14], **Frank Rücker**[14], **Konstanze Döhner**[14], **Hartmut Döhner**[14], **Jan Koster**[15], **Jan J. Molenaar**[15], **Rogier Versteeg**[15], **Marcel Kool**[2], **Uri Tabori**[5,12], **David Malkin**[12], **Andrey Korshunov**[8], **Michael D. Taylor**[5,16], **Peter Lichter**[2,#,@], **Stefan M. Pfister**[2,4,#,@], and **Jan O. Korbel**[1,17,#,@]

[1]European Molecular Biology Laboratory (EMBL), Meyerhofstr. 1, 69117 Heidelberg, Germany [2]Division of Molecular Genetics, German Cancer Research Center (DKFZ), Im Neuenheimer Feld 280, 69120 Heidelberg, Germany [3]Division of Theoretical Bioinformatics, DKFZ, Im Neuenheimer Feld 280, 69120 Heidelberg, Germany [4]Department of Pediatric Oncology, Hematology and Immunology, University Hospital Heidelberg, Im Neuenheimer Feld 430, 69120 Heidelberg, Germany [5]The Arthur and Sonia Labatt Brain Tumor Research Centre, The Hospital for Sick Children Research Institute, University of Toronto, Ontario, M5G 1L7, Canada [6]Pediatric Neurosurgery, Catholic University Medical School, Largo Agostino Gemelli 8, 00168, Rome, Italy [7]Department of Pathology, The Hospital for Sick Children, Toronto, Ontario, M5G 1L7, Canada [8]Department of Neuropathology, University of Heidelberg, and Clinical Cooperation Unit Neuropathology, DKFZ, Im Neuenheimer Feld 220, 69120 Heidelberg, Germany [9]Institute for Neuropathology, Evangelisches Krankenhaus, Remterweg 2, 33617 Bielefeld, Germany [10]Cnopf'sche Kinderklinik, Children's Hospital, Nürnberg, Germany [11]Clinical Cooperation Unit Pediatric Oncology, DKFZ, Im Neuenheimer Feld 280, 69120 Heidelberg, Germany [12]Genetics and Genome Biology Program and Division of Hematology/Oncology, The Hospital for Sick Children, Department of Pediatrics, University of Toronto, Ontario, M5G 1X8, Canada [13]McGill University Health Centre, 2155 Guy Street, Montreal, Canada H3H 2R9 [14]Department of Internal Medicine III, University of Ulm, Albert-Einstein Allee 23, 89081 Ulm, Germany [15]Amsterdam Medical Center, Meibergdreef 9, 1105 AZ Amsterdam, The Netherlands [16]Division of

[@]To whom correspondence should be addressed: peter.lichter@dkfz-heidelberg.de, s.pfister@dkfz-heidelberg.de and jan.korbel@embl-heidelberg.de.
[*]These authors contributed equally.
[#]Joint senior authors.

ACCESSION NUMBERS

Sequence data analyzed in our study can be accessed from EGA (accession: EGAS00001000085) and microarray data from GEO (accessions: GSE14437, GSE32462, GSE19101, GSE23452, GSE34323, and GSE34258).

SUPPLEMENTAL INFORMATION

Supplemental Information includes 5 tables, 2 datasets, and 2 figures.

Neurosurgery, The Hospital for Sick Children, University of Toronto, Ontario, M5G 1X8, Canada
[17]European Bioinformatics Institute, Wellcome Trust Genome Campus, Hinxton, Cambridge, CB10 1SD, UK

SUMMARY

Genomic rearrangements are thought to occur progressively during tumor development. Recent findings, however, suggest an alternative mechanism, involving massive chromosome rearrangements in a one-step catastrophic event termed chromothripsis. We report the whole-genome sequencing-based analysis of a Sonic-Hedgehog medulloblastoma (SHH-MB) brain tumor from a patient with a germline *TP53* mutation (Li-Fraumeni syndrome), uncovering massive, complex chromosome rearrangements. Integrating *TP53* status with microarray and deep sequencing-based DNA rearrangement data in additional patients reveals a striking association between *TP53* mutation and chromothripsis in SHH-MBs. Analysis of additional tumor entities substantiates a link between *TP53* mutation and chromothripsis, and indicates a context-specific role for p53 in catastrophic DNA rearrangements. Among these, we observed a strong association between somatic *TP53* mutations and chromothripsis in acute myeloid leukemia. These findings connect p53 status and chromothripsis in specific tumor types, providing a genetic basis for understanding particularly aggressive subtypes of cancer.

INTRODUCTION

Li-Fraumeni syndrome (LFS, OMIM #151623) is an autosomal dominant hereditary disorder that is associated with a greatly increased susceptibility to cancer (Li and Fraumeni, 1969). Most LFS patients harbor heterozygous germline mutations of *TP53*, the gene encoding the p53 tumor suppressor (Malkin et al., 1990). Mutant p53 can prime cells for tumor development due to aberrant cell cycle control and DNA damage response signals, and a failure to induce cell cycle arrest, senescence or apoptosis (Forbes et al., 2011; Vogelstein et al., 2000).

In a pilot study within the International Cancer Genome Consortium (ICGC) Pediatric Brain Tumor Research Project (www.pedbraintumor.org) we analyzed a medulloblastoma and paired normal sample from an LFS patient by whole-genome sequencing. Medulloblastoma is the most common malignant brain tumor of childhood, and the malignancy causing the highest cancer-related mortality in children. Medulloblastoma belongs to the spectrum of recognized LFS tumors (Taylor et al., 2000). Recent molecular studies have revealed that medulloblastoma comprises at least four distinct sub-entities, which differ in terms of cell-of-origin, clinicopathologic features, and disease outcome (Cho et al., 2011; Gibson et al., 2010; Kool et al., 2008; Northcott et al., 2011b; Remke et al., 2011). The investigated patient had a Sonic-Hedgehog subtype medulloblastoma (SHH-MB), a tumor arising from the external granular layer cells of the cerebellum (Bühren et al., 2000; Wechsler-Reya and Scott, 1999). SHH-MBs form the clinically and histopathologically most heterogeneous medulloblastoma subtype, making it challenging to predict response to therapy and patient outcome solely based on subtype affiliation (Northcott et al., 2011a; Remke et al., 2011). Cancer genome sequencing efforts underway will likely enable further refinements in medulloblastoma subtype classification, and provide novel molecular signatures for patient stratification.

Unexpectedly, the tumor genome showed massive genomic rearrangements consistent with a reshuffling of genetic material from individual chromosomes, in keeping with the recently proposed chromothripsis model for tumorigenesis (Greek; *chromo* from chromosome; *thripsis*, for shattering into pieces; Stephens et al., 2011). Chromothripsis, which is thought

to occur in 2–3% of cancers (with an incidence of ~25% in bone cancers; Stephens et al., 2011), involves the acquisition of numerous rearrangements through a single catastrophic event, fundamentally different from the stepwise (progressive) acquisition of alterations by tumor cells (Fearon and Vogelstein, 1990; Nowell, 1976). In this study, we integrate whole genome sequencing and array-based approaches to further characterize this rearrangement phenomenon, and discover a novel link between chromothripsis and *TP53* mutations, providing evidence that the status of p53 can influence catastrophic DNA rearrangements in a cell context-specific manner.

RESULTS

Whole-genome sequencing of a medulloblastoma in a Li-Fraumeni syndrome patient revealed highly complex DNA rearrangements

We initially analyzed an SHH-MB and paired normal tissue sample from a female LFS patient (LFS-MB1), who harbored a hereditary *TP53* mutation (Table S1) predicted to eliminate p53 DNA binding activity (Rieber et al., 2009). We performed whole-genome paired-end sequencing followed by DNA sequence variant discovery (Table 1). We searched for single nucleotide variants (SNVs) by directly evaluating the alignment of DNA reads onto the human reference genome (Depristo et al., 2011; Li et al., 2009) and identified large-scale rearrangements by paired-end mapping (Korbel et al., 2007), split-read analysis (Ye et al., 2009), and read-depth analysis (Abyzov et al., 2011; Chiang et al., 2009; Waszak et al., 2010).

The inherited *TP53* mutation was detected in both tissue samples. Furthermore, we identified 24 tumor-specific SNVs that were predicted to alter protein-coding sequences (Tables 1, S1 and Figure 1A). This is slightly more than was observed in a recent study focusing on exonic regions in sporadic medulloblastomas (average 5.7 non-synonymous SNVs per sample; range 1–17 (Parsons et al., 2011)). These differences could reflect an increased genome-wide mutation rate in LFS patients or could be the result of a comparably higher sensitivity of our whole-genome sequencing approach. Using PCR we verified 20 out of 21 SNVs for which PCR primers could be designed (>95%). We did not observe any somatic small insertions or deletions (<50bp) in protein-coding regions. However, we uncovered numerous large (up to megabase-scale) alterations in the tumor sample. Amongst these were distinct amplifications of SHH pathway members (*MYCN* and *GLI2*), which we verified by fluorescence *in situ* hybridization (FISH), and a somatic loss of the wild-type *TP53* allele by deletion of the 17p chromosome arm (Table S1, Figure 1E).

The most striking feature in LFS-MB1, however, was a pattern of complex somatic rearrangements that was markedly different from aberrations that we, and others have previously described in medulloblastoma (Cho et al., 2011; Northcott et al., 2009; Pfister et al., 2009). This included multiple highly amplified genomic segments, which were clustered on individual chromosome arms (Figure 1A), resulting in frequent alternations between a normal disomic copy-number state and an extreme state with a segmental copy-number of up to 30. On chromosome 3, three segments were highly amplified, whereas on chromosome 4, six segments were amplified and on chromosome 14, four segments were amplified. Based on the mapping of sequenced paired-ends, we determined physical connections linking the amplified sequences on chromosome 3 (intra-chromosomal), as well as the amplified segments from chromosomes 4 and 14 (inter-chromosomal). Strikingly, the amplified fragments from chromosomes 4 and 14 appeared fused together to form a circular 1.2Mb extra-chromosomal structure (so-called “double minute” chromosome) consisting of a complex medley of inter- and intra-chromosomal junctions (Figure 1B). Using PCR, we verified a series of these connections, including all four inter-chromosomal links (Figure 1C, Table S1). FISH experiments also confirmed the predicted co-localization of highly

amplified segments on chromosome 3, indicating that these fragments formed yet another double minute chromosome (Figures 1D, S1), as predicted by the sequencing data.

It is unlikely that these extrachromosomal structures occurred as a consequence of progressive genomic alterations. Double minute chromosomes have been described to typically encompass segments from confined genomic regions, rather than from several distinct regions of a chromosome or multiple chromosomes (Storlazzi et al., 2010). The recently described *chromothripsis* phenomenon, however, may explain the observed complex rearrangements, as this phenomenon can lead to the formation of double minute chromosomes containing fragments from multiple regions (Stephens et al., 2011). The chromothripsis model can further explain the strikingly similar, alternating copy-number states of adjacent amplicons and the medley of relative orientations with which DNA fragments rearranged.

DNA copy-number profiling of additional medulloblastomas reveals a link between *TP53* mutations and chromothripsis in SHH-MB

Previous studies have shown that evidence for chromothripsis can be inferred from SNP microarray-based DNA copy-number profiles (Stephens et al., 2011). To assess the occurrence of chromothripsis in a broader series, we analyzed SNP array data from 98 medulloblastomas, including samples from all four molecular subtypes (Table S2). We also carried out *TP53* sequencing in all tumors. Specifically, we analyzed 73 samples with previously published SNP array data (Northcott et al., 2009), and generated additional SNP array data for 25 tumors, including nine with known *TP53* mutations. To infer the occurrence of chromothripsis, we required at least 10 changes in segmental copy-number involving two or three distinct copy-number states on a single chromosome (see Experimental Procedures).

The vast majority of tumors displayed considerably fewer than ten copy-number state changes per chromosome (Figure 2, Data S1). A subset of cases, however (13/98), showed rearrangements consistent with chromothripsis (Figure 2, Data S1). Notably, eleven of these thirteen cases were SHH-MBs, and ten out of the eleven SHH-MBs harbored *TP53* mutations, whereas three cases (including one SHH-MB and two Group 4 subtype medulloblastomas) displayed a single copy *TP53*-loss through hemizygous 17p deletion (Figure 2). Strikingly, all (10/10) SHH-MBs with mutant *TP53* displayed rearrangements consistent with chromothripsis, whereas none (0/22) of the wild-type (*TP53*+/+) SHH-MBs showed evidence for chromothripsis (Figure 2, Data S1). This difference is highly significant ($p=1.6\times10^{-8}$, two-tailed Fisher's exact test), indicating that mutant *TP53* is strongly associated with chromothripsis in SHH-MB.

The ten mutant *TP53* tumors with chromothripsis included two cases with heterozygous *TP53* mutation (*TP53*+/m) and eight cases with loss of the wild-type *TP53* allele (*TP53*m/−). By comparison, only one of three SHH-MBs in our cohort harboring a *TP53*+/− genotype (hemizygous 17p deletion) showed rearrangements consistent with chromothripsis. Whereas *TP53* mutation can impair or reduce the function of p53 due to dominant negative activity, hemizygous *TP53* deletion may not have as significant an effect on protein function, since p53 expression levels are primarily regulated post-translationally (reviewed in Vogelstein et al., 2000).

The other three medulloblastoma subtypes rarely or never displayed rearrangements consistent with chromothripsis. In the Group 4 medulloblastoma subtype, 2/26 cases showed a copy-number pattern consistent with chromothripsis (both in the context of hemizygous *TP53* deletion). In the Group 3 subtype, we did not observe evidence for chromothripsis amongst 26 analyzed tumors (Figure 2AB). No *TP53* mutations were observed in either

Group 3 or Group 4 tumors. WNT subtype tumors also did not display any evidence for chromothripsis (0/11), despite the known association of *TP53* mutations with this subgroup (Pfaff et al., 2010) and 4/11 cases harboring a *TP53* mutation. These results indicate that the link between p53 status and chromothripsis in medulloblastoma is context-specific.

The inferred association between *TP53* and chromothripsis in SHH-MB makes it tempting to hypothesize that these catastrophic DNA rearrangements may have occurred as a consequence of preceding *TP53* mutations. To examine whether other medulloblastoma patients with chromothripsis harbored germline mutations, we analyzed constitutional DNA samples for those *TP53* mutant cases where paired normal tissue was available. We were able to retrieve germline DNA for 3 of the 4 *TP53* mutated WNT tumors, and 6/10 *TP53* mutated SHH tumors. Strikingly, whereas the *TP53* mutations in the WNT group were all somatically acquired (3/3), most of the tested germline samples from the SHH group (5/6) harbored the same *TP53* alterations as their paired tumors. Thus, in addition to linking p53 status to complex chromosomal rearrangements, we also identified five previously undiagnosed LFS cases amongst the SHH-MBs showing chromothripsis, which we herein refer to as LFS-MB2 – LFS-MB6 (Table S2).

We used deep sequencing, followed by counting DNA reads that identify mutant or wild-type *TP53* alleles, to analyze the abundance of mutant *TP53* relative to wildtype *TP53* in several tumors. This analysis followed the rationale that a high mutant allele frequency can indicate an early mutational event, whereas a low frequency indicates late occurrence – an analysis that may facilitate an evaluation of cause *versus* consequence. We used this approach in four SHH-MBs with germline *TP53* mutation (LFS-MB1 – LFS-MB4), the SHH-MB with confirmed somatic *TP53* mutation and chromothripsis (MB2034), and two *TP53* mutated WNT medulloblastomas (Supplemental Experimental Procedures). The mutant allele frequencies of the LFS-associated SHH-MBs were 87–100% (Table S2), suggesting that loss of the wild-type *TP53* allele is typically an early event in SHH-MBs seen in LFS patients. Whereas the WNT subtype medulloblastomas showed comparably lower mutant *TP53* allele frequencies (35–48%), all (14/14; 100%) DNA reads of the SHH-MB tumor MB2034 mapped to the mutant *TP53* allele. Absence, or very low frequency, of the *TP53* wild-type allele suggests that the somatic *TP53* mutation likely occurred as a very early (possibly initiating) event during medulloblastoma tumorigenesis in MB2034.

DNA copy-number profiles of medulloblastoma mouse models substantiates the link between *TP53* and chromothripsis in SHH-MB

We further reanalyzed published microarray data from two SHH-MB mouse models. The mice were hemizygous for *patched* (Ptch+/−), which promotes the development of SHH-MB-like tumors (Buonamici et al., 2010; Ishida et al., 2010). One study examined tumor growth in mice receiving medulloblastoma tumors (allografts) from a donor mouse lacking the murine p53 ortholog (Trp53) and a copy of *patched* (Buonamici et al., 2010) whereas another study examined tumors from Ptch+/−;Trp53+/+ mice (Ishida et al., 2010). All six tumors in mice receiving allografts from the Ptch+/−;Trp53−/− donor showed rearrangements consistent with chromothripsis (Data S2). Chromosome 16 was affected in each case, suggesting that chromothripsis had occurred already in the donor. 2/6 recipient mice further acquired alterations consistent with chromothripsis on other chromosomes (Supplemental Experimental Procedures). By comparison, none (0/3) of the Ptch+/−;Trp53+/+ mice showed chromothripsis (Data S2). These findings provide additional support for a link between chromothripsis and p53 in SHH-MB.

Whole-genome sequencing of three additional *TP53* mutated SHH-MBs verifies the occurrence of chromothripsis

We next subjected SHH-MB and paired normal tissue samples from three of the newly identified LFS patients (LFS-MB2 – LFS-MB4) to additional analysis by whole-genome sequencing, using the same approach as with LFS-MB1. One case (LFS-MB3) was sequenced to a lower whole-genome coverage (Table 1) sufficient for confirming the presence of chromothripsis, complemented by deep sequencing of exonic regions using a targeted exome capture approach. To better facilitate a detailed characterization of the massive rearrangements seen in chromothripsis, we additionally used long-range paired-end mapping (Korbel et al., 2007), generating deep physical genomic coverage of the two samples for which sufficient DNA was available (Table 1).

We identified 11–24 non-synonymous somatic SNVs in the three tumor samples (Tables 1, S3, S4) – again higher than the rate previously reported in sporadic medulloblastoma (Parsons et al., 2011). The only recurrently altered gene we identified was *TP53*, which was confirmed to be mutated in the germline in all cases. Importantly, the genome sequencing data further verified the SNP array-based inference of chromothripsis in all tumors. Specifically, LFS-MB2 showed chromothripsis on chromosomes 3 and X, with resulting amplicons that were physically connected to form a complex double minute chromosome (Figure 3AB). Furthermore, chromosomes 8 and 17 displayed multiple alternations between few copy-number states, involving a crisscrossing between one, two and three copies (Figure 3A) – a rearrangement pattern that is also typical for chromothripsis (Stephens et al., 2011). In LFS-MB3, chromosome 15 displayed one of the most striking genomic alteration patterns in our sample set, with >100 highly-rearranged segments (Figure 3D). LFS-MB4 showed rearrangements consistent with chromothripsis on chromosomes 2 and 12, with several of the chromosome 2 segments forming another double minute chromosome (Figure 4AB).

We performed experimental validations, overall 27 PCRs and 3 FISH experiments, on all four SHH-MBs in which we carried out whole-genome sequencing. These experiments verified the chromothripsis-associated rearrangements inferred by paired-end mapping (Figures 1, 3, 4, S2). The FISH experiments further confirmed the presence of double minute chromosomes in nearly all tumor cells. In conjunction with the high magnitude of log-ratio shifts in the context of single-copy alterations resulting from chromothripsis (Figure 3AD, 4A, Data S1), this finding indicates an early occurrence of chromothripsis in SHH-MB tumorigenesis rather than a later, sub-clonal event.

Known medulloblastoma oncogenes are frequently amplified as a result of chromothripsis

Given the high incidence of chromothripsis in LFS-associated SHH-MB, we speculated that this phenomenon is a key driver of SHH-MB tumorigenesis. We observed an enrichment of oncogenes (2.3-fold enrichment; $P<0.03$; Fisher's exact test), and more specifically of oncogenes involved in SHH signaling (30-fold enrichment; $P<0.0002$; see Table 2), amongst highly amplified segments rearranged by chromothripsis. The abundance of oncogenes likely explains the observed high copy-numbers of rearranged structures such as double minute chromosomes – presumably resulting from unequal segregation during cell division and subsequent selection for a growth advantage of malignant cells.

Notably, in LFS-MB4 the chromothripsis-associated rearrangements brought two SHH signaling genes on chromosome 2 – *i.e.*, *MYCN* and *GLI2* – into close proximity (Figure 4). This pattern is in contrast to LFS-MB1, where the SHH-MB oncogenes *MYCN* and *GLI2* were amplified in different tumor cell subpopulations, and where chromosome 2 was not

affected by chromothripsis (Figure 1). Furthermore, in LFS-MB1 we observed another SHH signaling gene, *BOC*, amplified in association with chromothripsis (Table 2 and Figure S1).

In two patients, the chromothripsis-associated rearrangements led to the formation of putative in-frame fusions involving genes previously reported to be dysregulated in cancer (Table 2, Figures 4B). One of these genes, *NEB*, was recently reported to harbor somatic point mutations in medulloblastoma (Parsons et al., 2011), suggesting that the resulting fusion gene may play a crucial role in the respective tumor.

Characterization of the molecular nature of the catastrophic DNA rearrangements with complementary computational approaches

To further characterize these complex rearrangements we examined the visually apparent genomic clustering of amplified regions, which were frequently found on single chromosome arms, using computational simulations. We observed that segments contributing to inter-connected and highly amplified (>10-fold change in copy number) loci displayed pronounced topological clustering in all four sequenced SHH-MBs (Figure 5A), consistent with previous reports in the context of chromothripsis (Stephens et al., 2011).

Simulations were also used to evaluate the possibility that the observed patterns of vastly alternating normal disomic and “extreme” (highly amplified) copy-number states may be explained by progressive rearrangements. We analyzed chromosomes with inferred chromothripsis using 1000 simulations each, by progressively, and randomly, introducing all detected inter-segmental-connections that involved highly amplified regions into the respective patients’ germline background in a stepwise fashion (see Experimental Procedures). In all four cases, based on the results of the simulations, a progressive rearrangement model was rejected, thereby implicating the occurrence of chromothripsis. In each case the simulations resulted in less pronounced as well as less regular switches between copy-number states than the actual data ($p<0.005$; based on permutations; Figure 5B).

Analysis of breakpoint sequence signatures (Lam et al., 2010) revealed short microhomology tracts (≤4bp), compatible with non-homologous end-joining (NHEJ)-mediated double-strand repair, or microhomology-mediated break-induced replication (MMBIR) (Hastings et al., 2009a; Lee et al., 2007), for the vast majority of breakpoints (Figure 5C). In a few cases, short insertions of non-template DNA sequence were observed at the breakpoint junctions (Table S5). NHEJ-mediated repair of shattered DNA fragments appears more likely to be involved in this context, as it is difficult to reconcile the model of MMBIR with the massive rearrangements (including complex double minute chromosomes) we detected in association with chromothripsis. Furthermore, we did not identify templated insertions – commonly observed in association with replication-based rearrangement mechanisms (such as MMBIR) – at the breakpoint junctions of chromothripsis-associated rearrangements.

***TP53* mutation is linked to chromothripsis in acute myeloid leukemia—**To investigate a potential association between *TP53* mutations and chromothripsis in LFS-associated tumors other than medulloblastoma, we collected copy-number profile data for tumors from eleven LFS patients (Supplemental Experimental Procedures), including adrenocortical carcinoma ($n=4$), rhabdomyosarcoma ($n=4$), extrarenal rhabdoid tumor ($n=1$), neuroblastoma ($n=1$), and glioblastoma ($n=1$). In all eleven patients, DNA sequencing identified the presence of a *TP53* mutation in the germline. Four out of the eleven (36%) tumors showed rearrangements consistent with chromothripsis (Table S2 and Data S1). While larger sample sizes of these rare tumor entities are required for formal testing, our

results indicate that *TP53* germline mutations could be linked with a high incidence of chromothripsis in LFS-associated malignancies other than medulloblastoma.

The occurrence of chromothripsis in an SHH-MB with somatic *TP53* mutation led us to further investigate relationships between p53 and chromothripsis in other malignancies with available high-resolution SNP microarray and somatic *TP53* status. We obtained such data for acute myeloid leukemia (AML) (Parkin et al., 2010). Previous studies have reported that mutations in *TP53* correlate with "complex" karyotypes in AML (Haferlach et al., 2008). The *TP53* mutations in the AML patient cohort were somatically acquired as assessed using paired constitutional DNA (Parkin et al., 2010). Copy-number profiling revealed an abundance of massive, complex rearrangements in the *TP53* mutated AMLs, with numerous alternating copy-number state switches involving two or three copy-number states, that were specifically localized to single chromosomes (Figure 5D, Table S5). These rearrangements were markedly different from the pattern of general genomic instability observed in prototypical *TP53* mutated tumors (Data S2), and implicated chromothripsis in the tumorigenesis of *TP53* mutated AMLs. In total, 8/17 (47%) AMLs with a somatically acquired *TP53* mutant genotype, but only 1/91 (1%) AMLs with wild-type *TP53* (*TP53*+/+), displayed patterns of rearrangement consistent with chromothripsis, a finding that links somatic *TP53* mutations with chromothripsis in AML ($P=5.7 \times 10^{-7}$; Fisher's exact test).

We further analyzed a previously unpublished SNP microarray dataset from a cohort of 311 AML patients with available karyotypic subgrouping. These included 56 "complex" karyotype AMLs (Haferlach et al., 2008), 46% of which harbored *TP53* mutations, and an additional 18% of which harbored a *TP53*+/− genotype. Our analysis revealed a similar abundance of chromothripsis amongst *TP53* mutated tumors as in the aforementioned AML cohort. When applying our strict definition for inferring chromothripsis, approximately half of the *TP53* mutated tumors showed chromothripsis (Data S2, Table S5), while none of the cases classified as "non-complex" karyotype AML – which exhibit *TP53* mutations in only ~2% of cases (Haferlach et al., 2008) – harbored alterations resulting from chromothripsis. An additional 12% of *TP53* mutated AMLs harbored rearrangements reminiscent of chromothripsis that fell just below our conservative scoring threshold (Supplemental Experimental Procedures).

We additionally tested for enrichment of cancer-related genes in regions rearranged by chromothripsis in AML. In contrast to SHH-MBs, the AML samples did not harbor high-level amplifications in association with chromothripsis, and instead showed hemizygous deletions of tumor suppressors (Figure 5E), some of which have known roles in AML, including *FHIT*, *NBN*, and *IRF1* (Table S5). Further analysis of gene expression profiles in these AML samples (Supplemental Experimental Procedures) – including cases with and without evidence for chromothripsis – did not reveal evidence for SHH pathway activation (Data S2), as was seen in *TP53*-mutated SHH-MBs with chromothripsis. Thus, in AML chromothripsis is linked with somatically acquired *TP53* mutations, but not with SHH pathway activation.

The availability of clinical follow-up data for the AML patients also enabled us to test for an association of chromothripsis with poor prognosis. We tested for such an association in both aforementioned AML cohorts, controlling for patient age at diagnosis, since AMLs harboring "complex" karyotypes display an increased incidence in patients with advanced age (Mrozek, 2008). Indeed, we found that chromothripsis in AML is associated with poor survival ($P<0.0001$; Wald's test; Data S2), an association that remained significant independent from patient age, and "complex" karyotype classification, when assessed in multivariate analyses. These tests also revealed an increased age of diagnosis in *TP53*-mutated AMLs with chromothripsis (median=62 years (yr); mean=67 yr), compared to

TP53-mutated AMLs not showing chromothripsis (median=57 yr; mean=58 yr; *P*=0.04; KS-test).

DISCUSSION

Integrated analysis of DNA sequencing and microarray data enabled us to discover an association between mutations of a specific gene, *i.e. TP53*, with chromothripsis. The unexpected germline nature of mutant *TP53* in several LFS-associated SHH-MBs means that the *TP53* mutation must precede the massive shattering and chromosome rearrangements in these. This led us to propose a novel role for p53 in the initiation of, or cellular reaction to, chromothripsis – with *TP53* mutations predisposing cells for chromothripsis, or facilitating cell survival following catastrophic DNA rearrangements (Figure 6). The high frequency of *TP53* germline mutations specifically in SHH tumors further suggests that LFS patients may be predisposed to SHH-MB, rather than to medulloblastoma *per se*. This finding has clinical implications, and we recommend assessing the merit of testing SHH-MB patients with chromothripsis for germline *TP53* mutations, since regular screening in LFS families was recently shown to lead to a survival benefit (Villani et al., 2011). Additionally, particular care may be required with respect to current treatment regimens, which in most cases include DNA damaging agents and radiotherapy. These may induce therapy resistance in the primary tumor or trigger secondary malignancies in the context of constitutional *TP53* mutations and deficient DNA repair.

The frequent occurrence of chromothripsis in the context of germline alterations of *TP53* points to a possible requirement of *TP53* mutations in the tumor cell-of-origin, or of *TP53* mutations acquired early in tumor development. The identification of chromothripsis in the context of somatic *TP53* mutations in an SHH-MB patient and in several AMLs additionally implicates acquired, tumor-specific *TP53* mutations in chromothripsis.

Possible explanations for the absence of chromothripsis in several malignancies with *TP53* mutations, including several AMLs and WNT medulloblastomas, are: their comparably late acquisition of such mutations; the occurrence of *TP53* mutations in tumor subpopulations; and cell context-specific factors, including distinct gene expression programs. Further to this, selective growth advantages are likely to determine tumor development following chromothripsis. The higher rate of chromothripsis in *TP53*-mutated SHH-MBs (all cases we analyzed) compared to *TP53*-mutated AMLs (approximately half of the cases we analyzed) is striking. It is tempting to speculate that this difference is connected with the abundance of high-level oncogene amplifications, typically involving double minute chromosomes, in SHH-MBs with chromothripsis. The selective advantage of such oncogene amplification is likely higher than the selective advantage conferred by hemizygous tumor suppressor gene loss observed in AML. Furthermore, rare cases of chromothripsis in AMLs harboring wild-type *TP53*, and in medulloblastomas with hemizygous *TP53* deletion, show that chromothripsis can also occur in the absence of *TP53* point mutations – perhaps in association with low *TP53* gene dosage, or other genetic or epigenetic mechanisms causing p53 pathway dysregulation.

Our analyses of rearrangement breakpoints are in support of a model of massive DNA double strand breaks (Stephens et al., 2011), followed by NHEJ-mediated repair (Figure 6). The replication-associated mechanism MMBIR can also generate alterations with multiple breakpoints (Hastings et al., 2009a). The lack of templated insertions at the breakpoint junctions, however, which are thought to result from abortive attempts to use another template during replication (Hastings et al., 2009b; Howarth et al., 2011), does not substantiate the involvement of a replication-associated rearrangement mechanism in the complex alterations we observed.

Stephens et al. (2011) have discussed two possible scenarios that may underlie the chromosome shattering and rearrangement seen in chromothripsis. Both scenarios involve damage occurring in mitotic chromosomes, since the compaction of chromosomes during mitosis could explain the highly localized nature of the DNA breaks, which are often focused on a single chromosome. We note, however, that the known spatial organization of chromosomes maintained during interphase (Cremer and Cremer, 2001; Lichter et al., 1988) might similarly represent a structural basis for the local occurrence of DNA shattering. In one scenario, it was proposed by Stephens et al. that ionizing radiation may lead to a catastrophic series of DNA double strand breaks. Based on our observations, these breaks might be preferentially repaired by low-fidelity mechanisms, such as error-prone NHEJ, as these are known to play a greater role when levels of p53 activity are reduced (Dahm-Daphi et al., 2005). An additional result of impaired p53 activity could be an increased rate at which cells are able to survive, and divide, after acquiring catastrophic chromosome alterations.

In a second possible scenario, critical telomere shortening followed by chromosome end-to-end fusions (which are prone to occur in association with uncapped telomeres (Tusell et al., 2010)) and subsequent breakage could lead to chromothripsis. Furthermore, dividing cells with uncapped telomeres are delayed at the G2/M transition in a p53-dependent manner, and unprotected telomeres in p53-deficient cells undergoing mitosis were found to be shorter than average, and prone to form end-to-end fusions (Thanasoula et al., 2010). Intriguingly, LFS patients harbor shortened telomeres compared to unaffected individuals of the same age group, with average telomere length decreasing from generation to generation in affected families, and the age of onset of cancer showing an association with average telomere length (Tabori et al., 2007; Trkova et al., 2007). As two different chromosomes may participate in an end-to-end fusion, such events could explain our observations of chromothripsis leading to complex inter-chromosomal rearrangements (with derived double minute chromosomes), which involved no more than two chromosomes. Thus, critical telomere shortening followed by end-to-end fusions and subsequent tearing apart during mitosis provides a plausible explanation for the link between *TP53* mutations and chromothripsis reported in this study. The finding that chromothripsis frequently occurred in individuals with advanced age at diagnosis in *TP53*-mutant AML is also of note, given the progressive shortening of telomeres with age.

Additional contributions of p53 in controlling the G2/M transition checkpoint (Kastan and Bartek, 2004) suggest that the involvement of a different mechanism – premature chromosome compaction – may also be a possibility. In this process chromosomes from an S-phase nucleus condense prematurely and, as a result, may become shattered (Meyerson and Pellman, 2011). Given the multiple and varied roles that have been assigned to p53, it is possible that the link between *TP53* and chromothripsis is associated with more than one of the aforementioned functions acting in concert (Figure 6).

In contrast to earlier reports on the rarity of chromothripsis (Kloosterman et al., 2011; Stephens et al., 2011), we found that in specific biological contexts this phenomenon occurs at high frequency. In conclusion, results from our study – which reported the first whole-genome sequence data for tumors from LFS patients and for pediatric brain tumors – indicate a new role for p53, a protein also known as the ‘guardian of the genome’. Results from upcoming large-scale cancer genome sequencing studies (The International Cancer Genome Consortium, 2010) may shed light on additional factors associated with this catastrophic genomic phenotype.

EXPERIMENTAL PROCEDURES

Patients

Informed consent and an ethical vote (Institutional Review Board) were obtained according to ICGC guidelines (www.icgc.org). No patient underwent chemotherapy or radiotherapy prior to the surgical removal of the primary tumor.

DNA library preparation and sequencing

DNA library preparation was carried out using Illumina, Inc., paired-end (PE) and mate-pair (MP, or long-range paired-end mapping) protocols. In brief, 5ug (PE) or 10ug (MP) of genomic DNA isolations were fragmented to ~300bp (PE) insert-size with a Covaris device, or to ~4kb (MP) with a Hydroshear device, followed by size selection through agarose gel excision. Deep sequencing was carried out with Genome Analyzer IIx and HiSeq2000 instruments. Exome capturing was carried out with Agilent SureSelect Human All Exon 50 Mb in-solution capture reagents (vendor's protocol v2.0.1).

Sequence variant discovery and analysis

We mapped DNA read data onto the human reference genome and subsequently detected SNVs, InDels, and genomic rearrangements with complementary computational approaches (see Supplemental Experimental Procedures).

SNP arrays

SNP arrays were hybridized, and copy-number alterations identified, as previously described (Northcott et al., 2009). We inferred chromothripsis in cases where at least ten switches between two or three copy-number states were apparent on an individual chromosome – *e.g.*, a sequence of the states '2' and '1' ('*2; 1; 2; 1; 2; 1; 2; 1; 2; 1; 2'*), or ten switches between '2' and a highly amplified (e.g. '30') state ('*2; 30; 2; 30; 2; 30; 2; 30; 2; 30; 2'*). We chose this threshold as we and others have demonstrated that whereas sporadic medulloblastomas display a high degree of variability in the level of observed copy number alterations, specific patterns of alternating copy-number patterns with multiple breakpoints localized on one chromosome, involving few copy-number states, have not previously been described in these (Cho et al., 2011; Northcott et al., 2009; Pfister et al., 2009).

PCR validation

PCR validations for breakpoint junctions were performed as previously described (Korbel et al., 2007). SNVs were validated by PCR, followed by capillary sequencing in whole genome amplified (Qiagen) DNA samples.

FISH

FISH was performed as previously described (Pfister et al., 2009).

Breakpoint clustering simulation

To evaluate topographical clustering of chromothripsis-associated DNA segments we shuffled the location of amplicons (>10-fold change in copy number) along single chromosomes, using 1000 simulations each. We limited our simulations to mappable regions of the reference genome (*i.e.*, genomic segments where >50% of the DNA reads could be uniquely aligned).

Rearrangement formation mechanism analysis

Rearrangement mechanisms were inferred with BreakSeq (Lam et al., 2010), using recently described classification parameters (Mills et al., 2011).

Simulations of the progressive rearrangement model

We simulated progressively occurring alterations based on a recently formulated computational approach (Stephens et al., 2011), as described in detail in the Supplemental Experimental Procedures.

Cancer gene enrichment analysis

Lists of cancer-related genes associated with SHH-MB and AML were compiled by supplementing a curated general cancer gene set with comprehensive lists of previously published disease-specific genes (see Table S5 and Supplemental Experimental Procedures). We then assessed whether these gene sets were enriched in regions affected by chromothripsis compared to the whole set of RefSeq genes, using Fisher's exact test.

Supplementary Material

Refer to Web version on PubMed Central for supplementary material.

Acknowledgments

We thank Bettina Haase, David Ibberson, and Dinko Pavlinic from the EMBL GeneCore sequencing team for excellent support, and Matthias Hentze and Lars Steinmetz for valuable comments on earlier versions of the manuscript. High-performance computing facilities at EMBL and DKFZ supported the study technically. The project was supported by grants from the German Cancer Aid (109252) and the BMBF (ICGC 'PedBrain' Tumor Project; to P.L., S.M.P., A.K., R.E., B.B., O.W., and J.O.K.; and 01GS0871; to L.B., K.D., and H.D.), the European Commission (Health-F2-2010-260791, to JOK), the NIH (R01CA148699b) and the Pediatric Brain Tumor Foundation (to MDT), the Canadian Institutes for Health Research (MOP-97834, to DM), and the German Research Foundation (BU 1339/3-1, to LB, and KO 4037/1-1, to JOK).

References

Abyzov A, Urban AE, Snyder M, Gerstein M. CNVnator: an approach to discover, genotype, and characterize typical and atypical CNVs from family and population genome sequencing. Genome Res. 2011; 21:974–984. [PubMed: 21324876]

Bühren J, Christoph AH, Buslei R, Albrecht S, Wiestler OD, Pietsch T. Expression of the neurotrophin receptor p75NTR in medulloblastomas is correlated with distinct histological and clinical features: evidence for a medulloblastoma subtype derived from the external granule cell layer. J Neuropathol Exp Neurol. 2000; 59:229–240. [PubMed: 10744061]

Buonamici S, Williams J, Morrissey M, Wang A, Guo R, Vattay A, Hsiao K, Yuan J, Green J, Ospina B, et al. Interfering with resistance to smoothened antagonists by inhibition of the PI3K pathway in medulloblastoma. Sci Transl Med. 2010; 2:51ra70.

Chiang DY, Getz G, Jaffe DB, O'Kelly MJ, Zhao X, Carter SL, Russ C, Nusbaum C, Meyerson M, Lander ES. High-resolution mapping of copy-number alterations with massively parallel sequencing. Nat Methods. 2009; 6:99–103. [PubMed: 19043412]

Cho YJ, Tsherniak A, Tamayo P, Santagata S, Ligon A, Greulich H, Berhoukim R, Amani V, Goumnerova L, Eberhart CG, et al. Integrative genomic analysis of medulloblastoma identifies a molecular subgroup that drives poor clinical outcome. J Clin Oncol. 2011; 29:1424–1430. [PubMed: 21098324]

Cremer T, Cremer C. Chromosome territories, nuclear architecture and gene regulation in mammalian cells. Nat Rev Genet. 2001; 2:292–301. [PubMed: 11283701]

Dahm-Daphi J, Hubbe P, Horvath F, El-Awady RA, Bouffard KE, Powell SN, Willers H. Nonhomologous end-joining of site-specific but not of radiation-induced DNA double-strand breaks is reduced in the presence of wild-type p53. Oncogene. 2005; 24:1663–1672. [PubMed: 15688024]

Depristo MA, Banks E, Poplin R, Garimella KV, Maguire JR, Hartl C, Philippakis AA, Del Angel G, Rivas MA, Hanna M, et al. A framework for variation discovery and genotyping using next-generation DNA sequencing data. Nat Genet. 2011; 43:491–498. [PubMed: 21478889]

Fearon ER, Vogelstein B. A genetic model for colorectal tumorigenesis. Cell. 1990; 61:759–767. [PubMed: 2188735]

Forbes SA, Bindal N, Bamford S, Cole C, Kok CY, Beare D, Jia M, Shepherd R, Leung K, Menzies A, et al. COSMIC: mining complete cancer genomes in the Catalogue of Somatic Mutations in Cancer. Nucleic Acids Res. 2011; 39:D945–950. [PubMed: 20952405]

Gibson P, Tong Y, Robinson G, Thompson MC, Currle DS, Eden C, Kranenburg TA, Hogg T, Poppleton H, Martin J, et al. Subtypes of medulloblastoma have distinct developmental origins. Nature. 2010; 468:1095–1099. [PubMed: 21150899]

Haferlach C, Dicker F, Herholz H, Schnittger S, Kern W, Haferlach T. Mutations of the TP53 gene in acute myeloid leukemia are strongly associated with a complex aberrant karyotype. Leukemia. 2008; 22:1539–1541. [PubMed: 18528419]

Hastings PJ, Ira G, Lupski JR. A microhomology-mediated break-induced replication model for the origin of human copy number variation. PLoS Genet. 2009a; 5:e1000327. [PubMed: 19180184]

Hastings PJ, Lupski JR, Rosenberg SM, Ira G. Mechanisms of change in gene copy number. Nat Rev Genet. 2009b; 10:551–564. [PubMed: 19597530]

Howarth KD, Pole JC, Beavis JC, Batty EM, Newman S, Bignell GR, Edwards PA. Large duplications at reciprocal translocation breakpoints that might be the counterpart of large deletions and could arise from stalled replication bubbles. Genome Res. 2011; 21:525–534. [PubMed: 21252201]

Ishida Y, Takabatake T, Kakinuma S, Doi K, Yamauchi K, Kaminishi M, Kito S, Ohta Y, Amasaki Y, Moritake H, et al. Genomic and gene expression signatures of radiation in medulloblastomas after low-dose irradiation in Ptch1 heterozygous mice. Carcinogenesis. 2010; 31:1694–1701. [PubMed: 20616149]

Kastan MB, Bartek J. Cell-cycle checkpoints and cancer. Nature. 2004; 432:316–323. [PubMed: 15549093]

Kloosterman WP, Guryev V, van Roosmalen M, Duran KJ, de Bruijn E, Bakker SC, Letteboer T, van Nesselrooij B, Hochstenbach R, Poot M, et al. Chromothripsis as a mechanism driving complex de novo structural rearrangements in the germline. Hum Mol Genet. 2011; 20:1916–1924. [PubMed: 21349919]

Kool M, Koster J, Bunt J, Hasselt NE, Lakeman A, van Sluis P, Troost D, Meeteren NS, Caron HN, Cloos J, et al. Integrated genomics identifies five medulloblastoma subtypes with distinct genetic profiles, pathway signatures and clinicopathological features. PLoS One. 2008; 3:e3088. [PubMed: 18769486]

Korbel JO, Urban AE, Affourtit JP, Godwin B, Grubert F, Simons JF, Kim PM, Palejev D, Carriero NJ, Du L, et al. Paired-end mapping reveals extensive structural variation in the human genome. Science. 2007; 318:420–426. [PubMed: 17901297]

Lam HY, Mu XJ, Stutz AM, Tanzer A, Cayting PD, Snyder M, Kim PM, Korbel JO, Gerstein MB. Nucleotide-resolution analysis of structural variants using BreakSeq and a breakpoint library. Nat Biotechnol. 2010; 28:47–55. [PubMed: 20037582]

Lee JA, Carvalho CM, Lupski JR. A DNA replication mechanism for generating nonrecurrent rearrangements associated with genomic disorders. Cell. 2007; 131:1235–1247. [PubMed: 18160035]

Li FP, Fraumeni JF Jr. Soft-tissue sarcomas, breast cancer, and other neoplasms. A familial syndrome? Ann Intern Med. 1969; 71:747–752. [PubMed: 5360287]

Li H, Handsaker B, Wysoker A, Fennell T, Ruan J, Homer N, Marth G, Abecasis G, Durbin R. The Sequence Alignment/Map format and SAMtools. Bioinformatics. 2009; 25:2078–2079. [PubMed: 19505943]

Lichter P, Cremer T, Borden J, Manuelidis L, Ward DC. Delineation of individual human chromosomes in metaphase and interphase cells by in situ suppression hybridization using recombinant DNA libraries. Hum Genet. 1988; 80:224–234. [PubMed: 3192212]

Malkin D, Li FP, Strong LC, Fraumeni JF Jr, Nelson CE, Kim DH, Kassel J, Gryka MA, Bischoff FZ, Tainsky MA, et al. Germ line p53 mutations in a familial syndrome of breast cancer, sarcomas, and other neoplasms. Science. 1990; 250:1233–1238. [PubMed: 1978757]

Meyerson M, Pellman D. Cancer genomes evolve by pulverizing single chromosomes. Cell. 2011; 144:9–10. [PubMed: 21215363]

Mills RE, Walter K, Stewart C, Handsaker RE, Chen K, Alkan C, Abyzov A, Yoon SC, Ye K, Cheetham RK, et al. Mapping copy number variation by population-scale genome sequencing. Nature. 2011; 470:59–65. [PubMed: 21293372]

Mrozek K. Cytogenetic, molecular genetic, and clinical characteristics of acute myeloid leukemia with a complex karyotype. Semin Oncol. 2008; 35:365–377. [PubMed: 18692687]

Northcott PA, Hielscher T, Dubuc A, Mack S, Shih D, Remke M, Al-Halabi H, Albrecht S, Jabado N, Eberhart CG, et al. Pediatric and adult sonic hedgehog medulloblastomas are clinically and molecularly distinct. Acta Neuropathol. 2011a; 122:231–240. [PubMed: 21681522]

Northcott PA, Korshunov A, Witt H, Hielscher T, Eberhart CG, Mack S, Bouffet E, Clifford SC, Hawkins CE, French P, et al. Medulloblastoma comprises four distinct molecular variants. J Clin Oncol. 2011b; 29:1408–1414. [PubMed: 20823417]

Northcott PA, Nakahara Y, Wu X, Feuk L, Ellison DW, Croul S, Mack S, Kongkham PN, Peacock J, Dubuc A, et al. Multiple recurrent genetic events converge on control of histone lysine methylation in medulloblastoma. Nat Genet. 2009; 41:465–472. [PubMed: 19270706]

Nowell PC. The clonal evolution of tumor cell populations. Science. 1976; 194:23–28. [PubMed: 959840]

Parkin B, Erba H, Ouillette P, Roulston D, Purkayastha A, Karp J, Talpaz M, Kujawski L, Shakhan S, Li C, et al. Acquired genomic copy number aberrations and survival in adult acute myelogenous leukemia. Blood. 2010; 116:4958–4967. [PubMed: 20729466]

Parsons DW, Li M, Zhang X, Jones S, Leary RJ, Lin JC, Boca SM, Carter H, Samayoa J, Bettegowda C, et al. The genetic landscape of the childhood cancer medulloblastoma. Science. 2011; 331:435–439. [PubMed: 21163964]

Pfaff E, Remke M, Sturm D, Benner A, Witt H, Milde T, von Bueren AO, Wittmann A, Schottler A, Jorch N, et al. TP53 mutation is frequently associated with CTNNB1 mutation or MYCN amplification and is compatible with long-term survival in medulloblastoma. J Clin Oncol. 2010; 28:5188–5196. [PubMed: 21060032]

Pfister S, Remke M, Benner A, Mendrzyk F, Toedt G, Felsberg J, Wittmann A, Devens F, Gerber NU, Joos S, et al. Outcome prediction in pediatric medulloblastoma based on DNA copy-number aberrations of chromosomes 6q and 17q and the MYC and MYCN loci. J Clin Oncol. 2009; 27:1627–1636. [PubMed: 19255330]

Remke M, Hielscher T, Korshunov A, Northcott PA, Bender S, Kool M, Westermann F, Benner A, Cin H, Ryzhova M, et al. FSTL5 is a marker of poor prognosis in non-WNT/non-SHH medulloblastoma. J Clin Oncol. 2011; 29:3852–3861. [PubMed: 21911727]

Rieber J, Remke M, Hartmann C, Korshunov A, Burkhardt B, Sturm D, Mechtersheimer G, Wittmann A, Greil J, Blattmann C, et al. Novel oncogene amplifications in tumors from a family with Li-Fraumeni syndrome. Genes Chromosomes Cancer. 2009; 48:558–568. [PubMed: 19378321]

Stephens PJ, Greenman CD, Fu B, Yang F, Bignell GR, Mudie LJ, Pleasance ED, Lau KW, Beare D, Stebbings LA, et al. Massive genomic rearrangement acquired in a single catastrophic event during cancer development. Cell. 2011; 144:27–40. [PubMed: 21215367]

Storlazzi CT, Lonoce A, Guastadisegni MC, Trombetta D, D'Addabbo P, Daniele G, L'Abbate A, Macchia G, Surace C, Kok K, et al. Gene amplification as double minutes or homogeneously staining regions in solid tumors: origin and structure. Genome Res. 2010; 20:1198–1206. [PubMed: 20631050]

Tabori U, Nanda S, Druker H, Lees J, Malkin D. Younger age of cancer initiation is associated with shorter telomere length in Li-Fraumeni syndrome. Cancer Res. 2007; 67:1415–1418. [PubMed: 17308077]

Taylor MD, Mainprize TG, Rutka JT. Molecular insight into medulloblastoma and central nervous system primitive neuroectodermal tumor biology from hereditary syndromes: a review. Neurosurgery. 2000; 47:888–901. [PubMed: 11014429]

Thanasoula M, Escandell JM, Martinez P, Badie S, Munoz P, Blasco MA, Tarsounas M. p53 prevents entry into mitosis with uncapped telomeres. Curr Biol. 2010; 20:521–526. [PubMed: 20226664]

The Cancer Genome Atlas Research Network. Comprehensive genomic characterization defines human glioblastoma genes and core pathways. Nature. 2008; 455:1061–1068. [PubMed: 18772890]

The International Cancer Genome Consortium. International network of cancer genome projects. Nature. 2010; 464:993–998. [PubMed: 20393554]

Trkova M, Prochazkova K, Krutilkova V, Sumerauer D, Sedlacek Z. Telomere length in peripheral blood cells of germline TP53 mutation carriers is shorter than that of normal individuals of corresponding age. Cancer. 2007; 110:694–702. [PubMed: 17567834]

Tusell L, Pampalona J, Soler D, Frias C, Genesca A. Different outcomes of telomere-dependent anaphase bridges. Biochem Soc Trans. 2010; 38:1698–1703. [PubMed: 21118150]

Villani A, Tabori U, Schiffman J, Shlien A, Beyene J, Druker H, Novokmet A, Finlay J, Malkin D. Biochemical and imaging surveillance in germline TP53 mutation carriers with Li-Fraumeni syndrome: a prospective observational study. Lancet Oncol. 2011; 12:559–567. [PubMed: 21601526]

Vogelstein B, Lane D, Levine AJ. Surfing the p53 network. Nature. 2000; 408:307–310. [PubMed: 11099028]

Waszak SM, Hasin Y, Zichner T, Olender T, Keydar I, Khen M, Stutz AM, Schlattl A, Lancet D, Korbel JO. Systematic inference of copy-number genotypes from personal genome sequencing data reveals extensive olfactory receptor gene content diversity. PLoS Comput Biol. 2010; 6:e1000988. [PubMed: 21085617]

Wechsler-Reya RJ, Scott MP. Control of neuronal precursor proliferation in the cerebellum by Sonic Hedgehog. Neuron. 1999; 22:103–114. [PubMed: 10027293]

Ye K, Schulz MH, Long Q, Apweiler R, Ning Z. Pindel: a pattern growth approach to detect break points of large deletions and medium sized insertions from paired-end short reads. Bioinformatics. 2009; 25:2865–2871. [PubMed: 19561018]

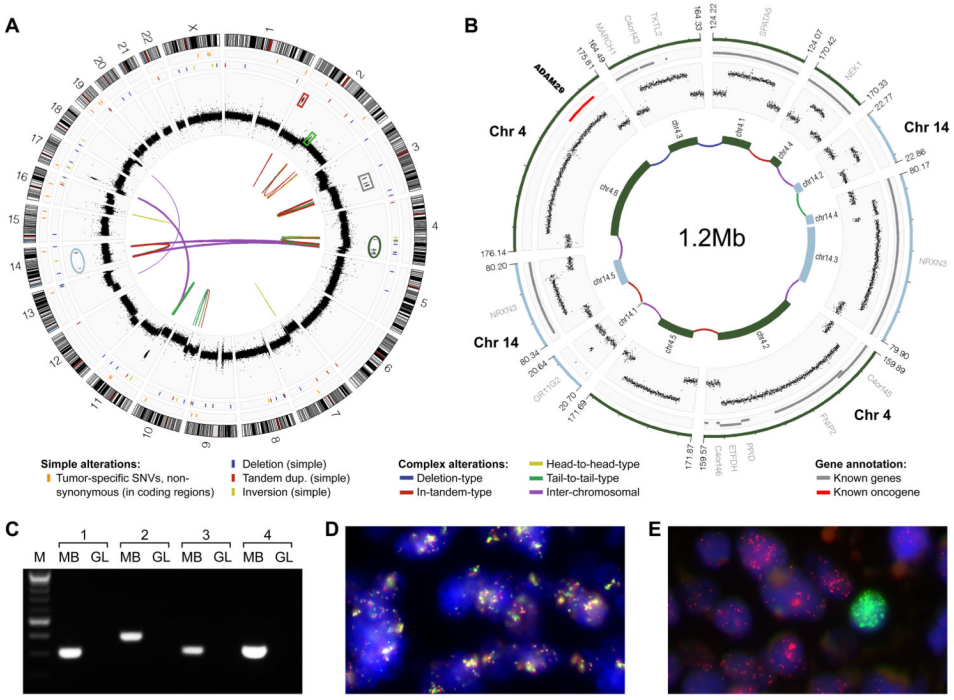

Figure 1.

Analysis of LFS-MB1 revealed catastrophic DNA rearrangements consistent with chromothripsis. (**A**) Genome-wide distribution of somatic DNA variants. Thin orange lines in outer-most panel are non-synonymous somatic SNVs; the next panel shows isolated genomic rearrangements. Read-depth plots (log_2-ratio tumor *vs.* germline), indicating copy-number alterations, are in black. Connecting lines show complex large-scale (e.g., inter-chromosomal) rearrangements identified by paired-end mapping. (**B**) Inferred double minute chromosome structure (originating segments from chromosome 4 and 14 are highlighted in panel (A)). Genes are in gray (known cancer genes are in red). (**C**) PCR validation of inter-chromosomal rearrangements contributing to the inferred double minute chromosome. MB, medulloblastoma; GL, germline. (**D**) FISH validation of rearrangements contributing to double minute chromosome derived from chromosome 3 segments. Probes match to normally distal regions of chromosome 3 (RP11-553D4, red, and RP11-265F19, light green; see panel (A) and Figure S1). (**E**) Amplification of *MYCN* (red) and *GLI2* (light green), not associated with chromothripsis (amplicon loci highlighted in panel (A) with red and light green boxes), was observed in distinct subpopulations of cells.

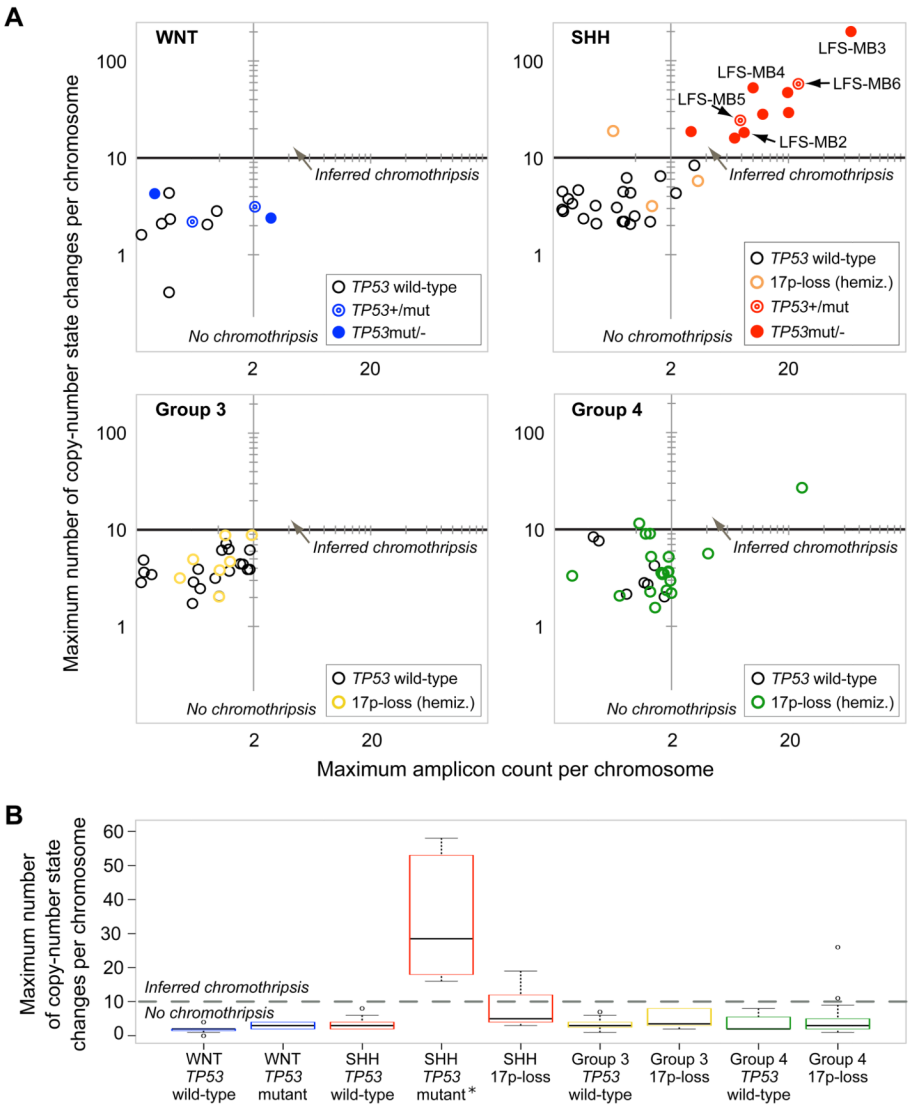

Figure 2.

SNP array copy-number profiles reveal a link between *TP53* mutation and chromothripsis in SHH-MB. (**A**) Maximum number of copy-number state changes, and amplicon counts, on most strongly affected (rearranged) chromosomes. Abbreviation: hemiz., hemizygous. Further details are available as Data S1. Random noise was added (*i.e.*, addition, or subtraction, of <0.5 copies) for visualization purposes. (**B**) Boxplot with maximum copy-number state changes on most strongly affected chromosome for different tumor subtypes and *TP53* statuses. *An outlying point observed in LFS-MB3 (>200 copy-number state changes) was omitted for visualization purposes.

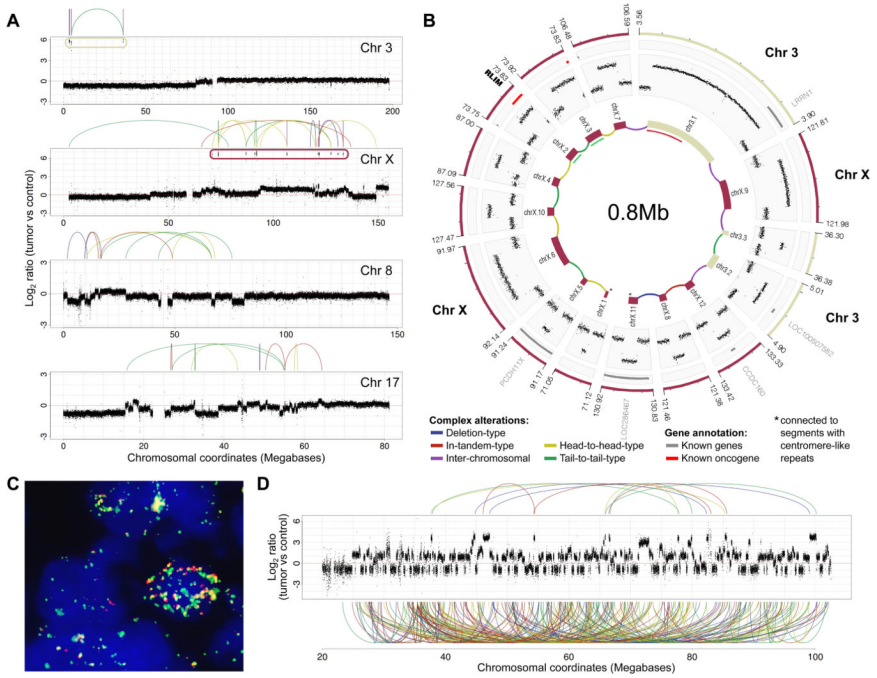

Figure 3.

Verification of chromothripsis in LFS-MB2 and LFS-MB3 by whole-genome sequencing. (**A**) Copy-number profiles in LFS-MB2. (**B**) Predicted double minute chromosome structure. *Segments connected to centromere-like repeat sequences. (**C**) FISH confirming co-localization of fragments from chromosomes 3 and X in LFS-MB2 (RP11-245A6, green and CTD-2530H13, red); positions of FISH probes are shown on the inner-most circle of panel (B)). PCR experiments also confirmed this co-localization (see Figure S2). (**D**) Read-depth plot showing chromosome 15 rearrangements resulting from chromothripsis in LFS-MB3. Links connecting amplified regions are displayed on top (other links involving rearranged segments are displayed at the bottom).

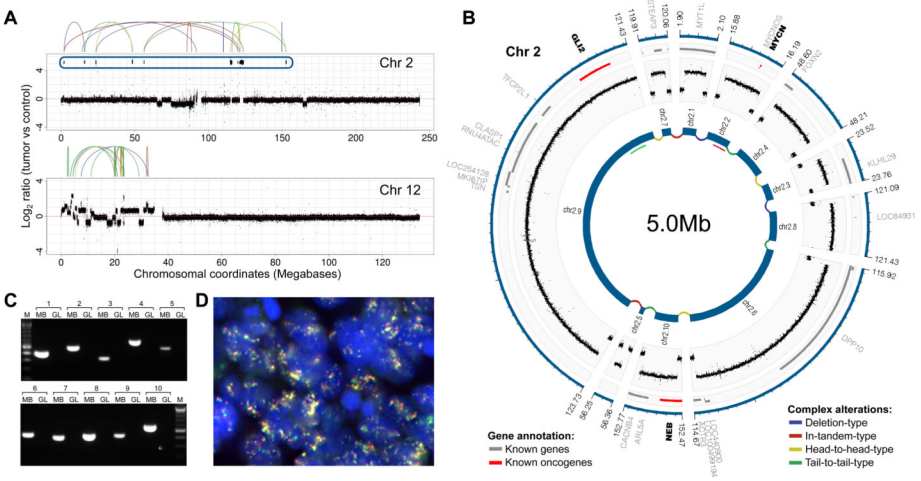

Figure 4.

Verification of chromothripsis in LFS-MB4. (**A**) DNA copy-number profiles. (**B**) Inferred double minute chromosome structure with SHH pathway members *MYCN* and *GLI2*. (**C**) PCR confirms juxtaposition of segments shown in panel (B). (**D**) FISH verifying co-localization of *MYCN* (red) and *GLI2* (green).

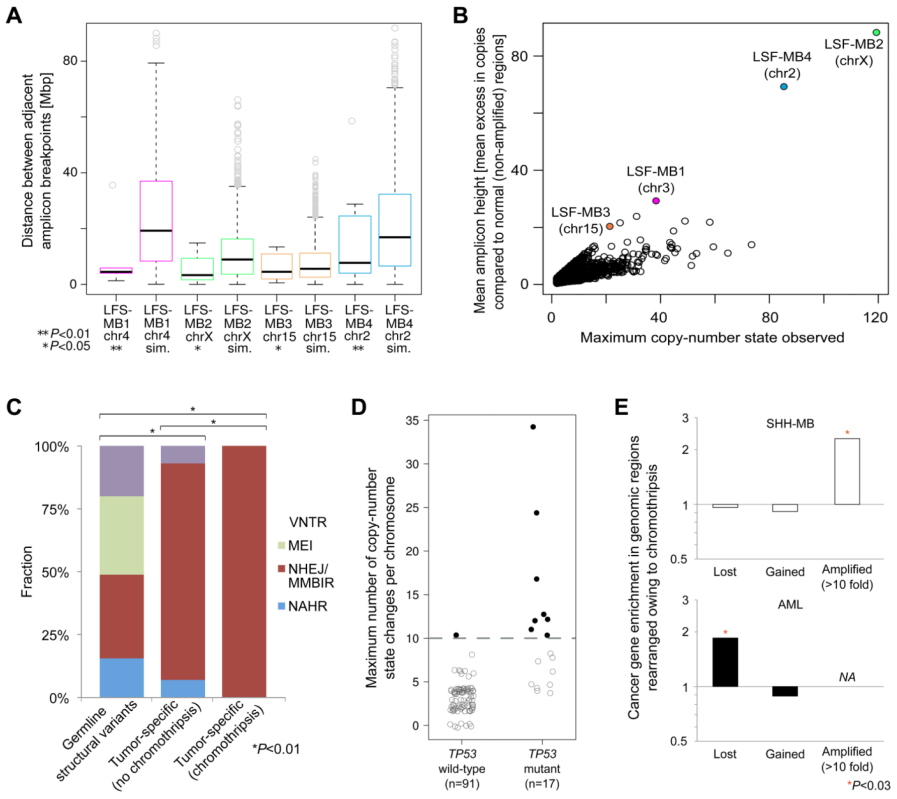

Figure 5.

Analysis of chromothripsis-associated DNA rearrangements in SHH-MB and AML. (**A**) Topographical clustering of amplified regions rearranged by chromothripsis. Sim., simulated amplicon distances (*P*-values are based on 1000 permutations). (**B**) Simulations of progressive rearrangements segregate from the actual data in terms of mean excess in copy-number compared to unaffected regions. (**C**) Rearrangement formation mechanisms analysis. Polymorphic genomic structural variants detected in the germline are shown for comparison. *P*-values, indicating significant differences between the distributions of inferred formation mechanisms, are based on Chi-square tests. VNTR, expansion or shrinkage of regions with variable number of tandem repeats; MEI, mobile element insertions; NAHR, non-allelic homologous recombination (other abbreviations: see main text). (**D**) Somatically acquired *TP53* mutations are linked with the occurrence of chromothripsis in AML. Black filled circles: AMLs with chromothripsis. Gray open circles: AMLs without chromothripsis. Example copy-number profiles are available as Data S2, and a detailed summary of the AML data is in Table S5. (**E**) Cancer gene enrichment in association with chromothripsis in SHH-MBs, analyzed by deep sequencing, and AMLs, analyzed by SNP arrays. Regions hemizygously deleted ('lost'), gained, and highly (>10-fold) amplified as a consequence of chromothripsis were separately analyzed. No genes displayed high-level amplification in AML in association with chromothripsis ('*NA*'). '*'significant based on Fisher's exact test.

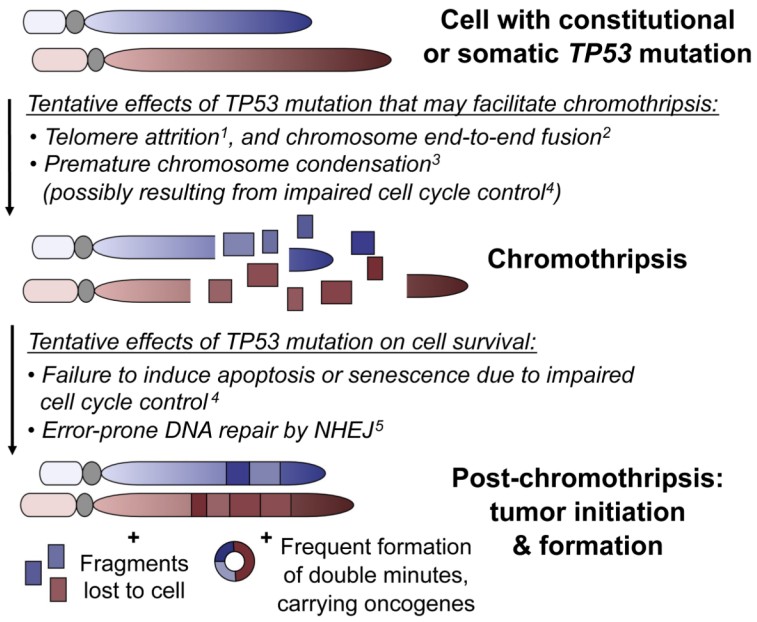

Figure 6.

New model linking *TP53* mutation status to catastrophic DNA rearrangements. Related references: [1]Tabori et al. (2007); [2]Tusell et al. (2010); [3]Meyerson and Pellman (2011); [4]Vogelstein et al. (2000); [5]Dahm-Daphi et al. (2005).

Table 1

Whole-genome sequencing and DNA sequence variant statistics

	LFS-MB1	LFS-MB2	LFS-MB3	LFS-MB4
Tumor bases sequenced	109×10^9	120×10^9	37×10^9	143×10^9
Paired normal tissue bases sequenced	116×10^9	125×10^9	17×10^9	114×10^9
Tumor physical coverage (span coverage)	43.5×	45.8×	77.8×	112.2×
Paired normal physical coverage	41.6×	51.6×	3.3×	49.5×
Tumor sequencing coverage	30.8×	34.6×	8.9×*	38.5×
Paired normal sequencing coverage	31.4×	36.7×	4.6×*	34.4×
Total somatic mutations (whole genome)	3,716	3,053	-	2,494
Non-silent coding mutations (val./tested)	24 (20/21)	22 (19/20)	18(−/−)*	11 (8/10)
Mutation rate per Mb	1.29	1.06	-	0.88

* In addition to whole-genome sequencing, whole-exome data was generated at 39× (tumor) and 37× (paired normal) coverage in this case.

'−', not assessed; val., validated.

Table 2

Chromothripsis-associated amplified regions typically contain medulloblastoma oncogenes

Chr	Name	Pathway/Process	Sample	Sources
4	*ADAM29*	Axonal Guidance Signaling	LFS-MB1	(1)
3	*BOC*	Sonic Hedgehog (SHH) signalling pathway	LFS-MB1	(2)
7	*CDK6*	Cell cycle: G1/S check point	LFS-MB2	(3)
2	*GLI2*	SHH signalling pathway	LFS-MB4	(2, 3)
15	*IGF1R*	Insulin-like growth factor 1 signalling	LFS-MB3	(3)
2	*MYCN*	MAPK- and SHH signalling pathway	LFS-MB4	(2, 3)
3	*NEK11*	intra-S DNA damage checkpoint	LFS-MB1	(3)
7	*NAMPT**	Nicotinate and Nicotinamide Metabolism	LFS-MB2	(3)
2	*NEB***	Striated Muscle Contraction	LFS-MB4	(1)

Shown are oncogenes in highly amplified genomic regions (>10-fold increased copy number) occurring in association with chromothripsis in SHH-MB. Sources: (1) Parsons et al. (2011); (2) SHH signalling pathway (manually curated); (3) cancer gene set curated by the Cancer Genome Atlas (The Cancer Genome Atlas Research Network, 2008).

* *NAMPT* is C-terminally fused to *CDK6*.

** *BEB* is N terminally fused to *ACTR3*. Chr, chromosome.